Available online at www.sciencedirect.com
ScienceDirect
Ceramics International 35 (2009) 1565–1568
CERAMICS INTERNATIONAL
www.elsevier.com/locate/ceramint

Synthesis of $LiMn_2O_4$ from a gelled ovalbumin matrix

T. Sri Devi Kumari, R. Kannan, T. Prem Kumar *

Electrochemical Power Systems Division, Central Electrochemical Research Institute, Karaikudi, Tamil Nadu 630006, India

Received 9 July 2008; received in revised form 17 July 2008; accepted 27 August 2008
Available online 5 October 2008

Abstract

A simple and inexpensive route for the preparation of $LiMn_2O_4$ using ovalbumin (egg white) as a gelating agent is described. Gelation of freshly extracted ovalbumin was effected by changes in ionic strength brought about by the addition of nitrate precursors to an aqueous solution of ovalbumin and subsequent warming. This resulted in tiny pockets of precursor materials getting trapped in the matrix of the gelled ovalbumin. Heat treatment of the gelled mass yielded submicron-sized $LiMn_2O_4$ crystals at temperatures as low as 400 °C.

Keywords: A. Sol–gel processes; D. Spinels; E. Batteries; Ovalbumin

1. Introduction

An important criterion that is often overlooked in the laboratory synthesis of cathode materials for lithium batteries is the viability of the process for large-volume production. Conventional solid-state fusion methods, involving repeated grinding, pelletizing and calcination, are energy-intensive and time-consuming. Problems of diffusion limitation associated with solid-state methods have been sought to be overcome by various elaboration methods [1–5]. A popular 'chemie doux' approach is the sol–gel method. In the sol–gel method, a sol, which is a suspension of small particulates dispersed in a liquid phase, is transformed into a gel, which is a viscous, three-dimensional polymeric network. A subsequent heat treatment of the gel yields the desired oxide. Often, the scope of sol–gel methods is extended to such preparative procedures that involve the transformation of a thick viscous liquid medium with no phase segregation into an amorphous glassy mass with no long-range networking. Conventional sol–gel preparative methods, however, cannot often be exploited at a commercial level because they usually employ expensive chemicals. Fine ceramic powders have thus been synthesized by use of water-soluble polymers mixed with precursor salts [6–8]. Water-soluble polymeric matrices used for such preparations include diethanolamine [6], triethanolamine [6], polyvinyl alcohol [6] and sucrose [6,7]. Recently, Dhara [9] used ovalbumin (egg white) as a water-soluble polymeric matrix to produce nanocrystalline alumina. In this paper, we describe the synthesis of submicron $LiMn_2O_4$ crystals from a stoichiometric mixture of lithium nitrate and manganese nitrate in ovalbumin.

2. Experimental

Freshly extracted egg white (165 ml) was homogenized in water (110 ml) by stirring on a magnetic stirrer. *n*-Octanol (2 ml) was added to this mixture as an antifoaming agent. $LiNO_3$ (20 mM) and $Mn(NO_3)_2{\cdot}4H_2O$ (40 mM), both from Merck, dissolved in 50 ml of water was added dropwise to the ovalbumin–water mixture with continuous stirring. After 2 h of stirring, the mixture turned homogeneous. The pH of the mixture, which was originally around 9, was now less than 3. The mixture was then allowed to gel by keeping in an oven overnight at 80 °C. The gelled mass was slowly vacuum-dried to a brown mass (precursor), charred at 200 °C, and calcined at 800 °C for 10 h.

The decomposition pattern of the precursor mass was followed by simultaneous thermogravimetric and differential thermal analyses (TA Instruments model SDT Q600) in air from room temperature to 800 °C. The heating rate was 5 °C/min. Structural characterization of the calcined products was done by a PANalytical model X'per PRO powder X-ray

* Corresponding author. Tel.: +91 4565 227550 to 227559; fax: +91 4565 227779.
E-mail addresses: premlibatt@yahoo.com, prem@cecri.res.in (T. Prem Kumar).

0272-8842/$34.00
doi:10.1016/j.ceramint.2008.08.020

diffractometer with nickel-filtered Cu Kα radiation between scattering angles of 10° and 80° in increments of 0.05°. Morphological features of the products were examined by scanning electron microscopy (Hitachi model S-3000H). Charge–discharge studies were carried out with coin cells assembled in standard 2032 stainless steel cell hardware. Lithium metal was used as the anode and a 1-M solution of $LiPF_6$ in EC:DEC (1:1, v/v) was used as the electrolyte. The cathode was prepared by blade-coating a slurry of 85 wt.% active material with 10 wt.% conductive carbon black and 5 wt.% PVdF binder in NMP on a stainless steel disc and drying the coating overnight at 120 °C in an oven. Cell assembly was done in an argon-filled glove box (MBraun MB-120G), which contained less than 2 ppm oxygen and moisture. The cells were cycled between 3.0 and 4.3 V at 0.1 C rate on a multi-channel battery tester (Arbin BT2000).

3. Results and discussion

3.1. Thermal analysis

As a gelling matrix for the preparation of oxide particles, ovalbumin possesses some desirable properties. It is inexpensive and available everywhere. It is also water-soluble, which means a homogeneous matrix for suspension of precursor salts can be made. The protein molecules in ovalbumin possess a net charge, which is dependent on solution pH. The charged sites favor association with cations in solution [10], and bind them to the gel structure. Ovalbumin is also easily amenable to gelling/denaturing by simple warming [11,12].

Fig. 1(a) shows the results of thermal analysis on the ovalbumin-salt precursor. A thermogram and a differential thermogram of salt-free ovalbumin are presented in Fig. 1(b) for comparison. In the case of ovalbumin, weight loss is considerable only at temperatures above 200 °C, suggesting that water molecules in albumin are strongly bonded to the protein molecules and that it takes higher energies to remove them. In contrast to the thermal behavior of ovalbumin, it can be seen from Fig. 1(a) that in the presence of added salts weight loss occurs from room temperature to about 370 °C in several steps. The final decomposition occurs between 395 and 425 °C, and there is no thermal event beyond 450 °C. The weight loss up to 120 °C is ascribed to superficial water loss as well as water loss from the hydration of $Mn(NO_3)_2{\cdot}4H_2O$, which begins to decompose at temperatures above 100 °C. There is an initial endotherm around 40 °C, which can be ascribed to the melting of $Mn(NO_3)_2{\cdot}4H_2O$ (mp 37 °C). There is also a gradual breakdown of structures and partial carbonization beyond 330 °C, a region where charring can be noticed. The charring process was accompanied by evolution of brown nitrogen dioxide, which became copious as the temperature rose to above 375 °C. A comparison of Fig. 1(a) and (b) shows that the final decomposition temperature is higher in the case of the ovalbumin–nitrate mixture, suggesting strong association of metal ions with the protein molecules. Both in Fig. 1(a) and (b), there is a broad endotherm before the final exothermic decomposition. Decomposition reactions are necessarily

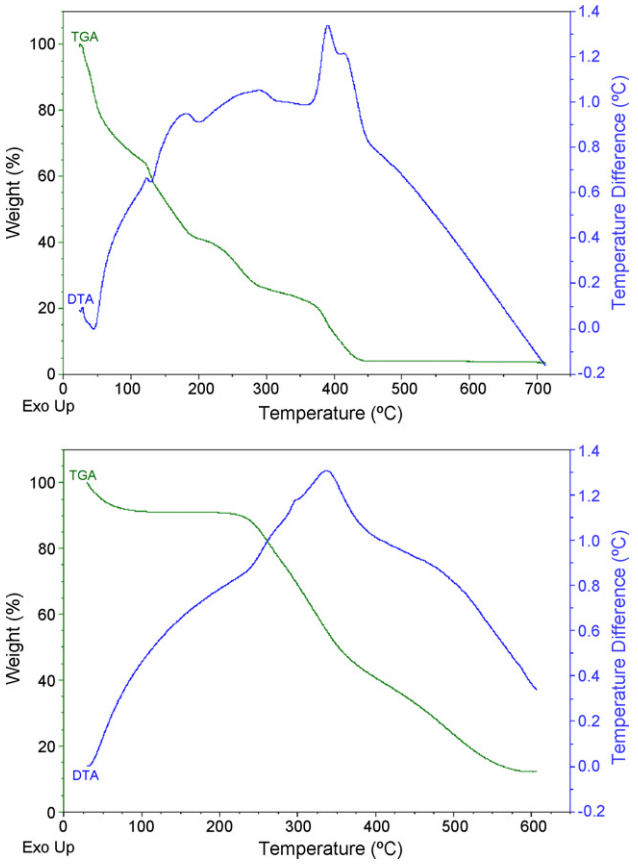

Fig. 1. TG and DTA profiles of (a) ovalbumin-salt precursor and (b) salt-free ovalbumin.

endothermic. This is because the system must absorb heat from its surroundings to raise its enthalpy to the critical limit of thermodynamic stability. It is beyond this critical limit that decomposition occurs. However, the decomposition of the high-energy molecules to form $LiMn_2O_4$ should, in principle,

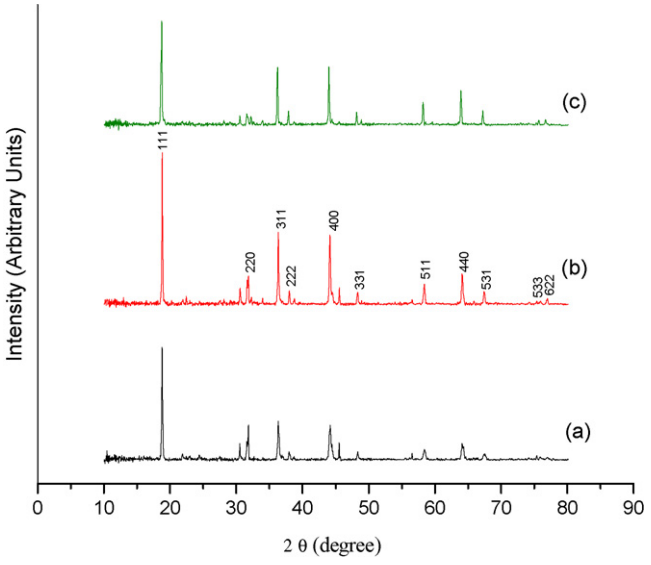

Fig. 2. Powder XRD patterns of $LiMn_2O_4$ calcined at (a) 700 °C, (b) 800 °C and (c) 900 °C for 10 h.

Table 1
Lattice parameters and crystallite sizes of $LiMn_2O_4$ prepared by 10-h calcinations at different temperatures.

Calcination temperature (°C)	Lattice parameter, a (Å)	Unit cell volume (Å^3)	Crystallite size (nm)	Peak intensity ratios	
				$I_{4\,0\,0}/I_{3\,1\,1}$	$I_{2\,2\,0}/I_{3\,1\,1}$
700	8.193	549.9	21.8	1.040	0.422
800	8.199	551.3	32.8	0.958	0.171
900	8.226	556.8	43.7	0.902	0.101

be exothermic, a fact reflected by the sudden rise in the differential thermogram towards the exothermic region.

3.2. X-ray diffraction

Powder XRD patterns recorded with the products obtained by 10-h calcination at 700, 800 and 900 °C are shown in Fig. 2. The patterns correspond to the cubic spinel structure in *Fd*3*m* space group of $LiMn_2O_4$. In fact, even a sample charred at around 400 °C showed such peaks, suggesting the high exothermicity of the combustion processes taking place [13]. The values of the lattice parameter a calculated from the XRD data are 8.193, 8.199 and 8.226 Å for samples calcined at 700, 800 and 900 °C, respectively (Table 1). The values are less than the 8.244 Å reported for $LiMn_2O_4$ synthesized by a solid-state method at 750 °C [14]. It is generally believed that the lattice parameter in the cubic spinel structure depends on the valence state of manganese. In insufficiently calcined products, a significant fraction of manganese ions are present in the Mn^{4+} state because of the greater stability of Mn^{4+} ions at low temperatures [15]. Therefore, the presence of larger amounts of the smaller Mn^{4+} ions (Mn^{4+}: 0.60 Å; Mn^{3+}: 0.68 Å [16]) leads to diminished values of a. With the replacement of part of the Mn^{4+} ions with Mn^{3+} ions at the higher temperatures, the cubic lattice parameter also increases.

3.3. SEM studies

Fig. 3 shows an SEM image of the $LiMn_2O_4$ product obtained by a 10-h calcinations at 800 °C. Stacks of sheets of crystalline $LiMn_2O_4$ of average sizes between 1 and 2 μm can be seen. However, the crystallite sizes of the $LiMn_2O_4$ particles, as calculated by using the Debye–Scherrer relation [17], which relates the full width at half maximum, FWHM, β, of an X-ray peak to its corresponding cos θ value by

$$\beta = \frac{\lambda}{\tau \cos\theta} \quad (1)$$

where λ is the incident X-ray wavelength, and τ is crystallite size, are 21.8, 32.8 and 43.7 nm, respectively, for the samples calcined at 700, 800 and 900 °C (Table 1), suggesting particle growth as the calcination temperature is raised.

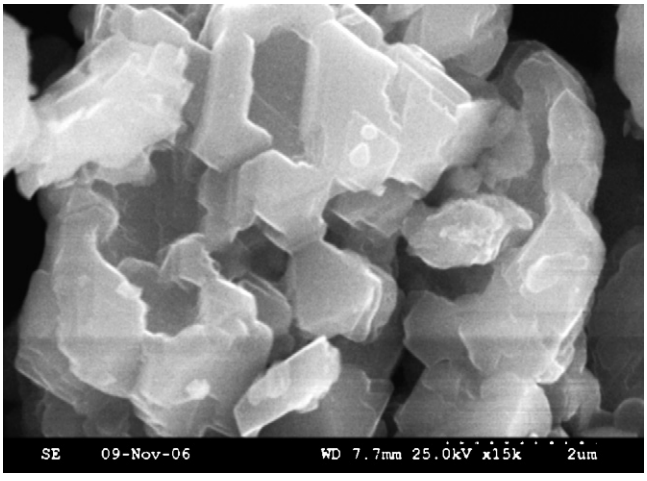

Fig. 3. An SEM image of $LiMn_2O_4$ calcined at 800 °C for 10 h.

3.4. Charge–discharge studies

The galvanostatic cycling performance of $LiMn_2O_4$ by 10-h calcination at different temperatures is depicted in Fig. 4. The highest first-cycle capacity of 127.0 mAh/g was obtained for the product calcined at 900 °C, while the lowest first-cycle capacity (120.2 mAh/g) was obtained with the sample calcined at 700 °C. This behavior is in accordance with the fact that the amount of Mn^{3+} ions in the sample increases with heat treatment [15]. However, the cyclability was the best for the sample calcined at 800 °C: the average capacity fades per cycle over the 30 cycles studied were 0.74, 0.40 and 0.86 mAh/g for samples calcined at 700, 800 and 900 °C, respectively. Moreover, the first-cycle capacity obtained with the 800 °C-calcined sample was also high, at 123.1 mAh/g. This suggests that a heat treatment protocol of 800 °C for 10 h was optimal. The present results favorably compare with those reported in the literature. For example, Fey et al. [18] showed that $LiMn_2O_4$ prepared with triethanolamine and starch as fuels under a temperature protocol of 10-h calcination at 800 °C gave a first-cycle capacity of 127 mAh/g between 3.0 and 4.3 V at 0.1 C rate. However, the capacity faded to 80% of its initial value (102 mAh/g) in a matter of 43 cycles, corresponding to an

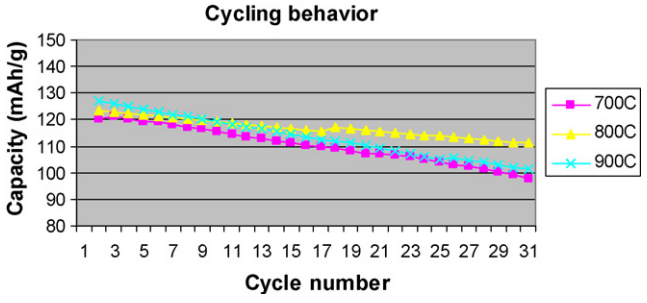

Fig. 4. Cycling behavior of $LiMn_2O_4$ calcined at 800 °C for 10 h.

average capacity fade of 0.58 mAh/g per cycle. It is thus clear that $LiMn_2O_4$ prepared with ovalbumin as a gelating agent has good electrochemical activity. Moreover, the method presents an inexpensive method for the preparation of battery-active oxidic materials.

The good performance of the sample calcined at 800 °C can be explained as follows. The structural integrity of $LiMn_2O_4$, which determines its performance as a lithium intercalating material, depends among other things on the site occupancy of the cations in the spinel structure. In the case of the ideal $LiMn_2O_4$ structure, the Mn^{3+} and Mn^{4+} ions are located in the 16*d* octahedral sites and the Li^+ ions in the 8*a* sites in a cubic close packed array of O^{2-} ions, which occupy the 32*e* sites [19–21]. However, the Li^+ ions show a propensity to occupy both 8*a* tetrahedral and 16*d* octahedral sites [22–24], which often leads to a partial replacement of manganese ions from their sites [23,24] by lithium ions. A small percentage of manganese ions have also been reported to be present in the 8*a* sites in Li–Mn–O spinels [16]. An important consideration in substitutional studies is the site occupancy of the substituent ions in the host matrix. Ohzuku et al. [21] used the integrated intensity ratios of close-lying peaks in the X-ray diffractogram to determine the extent of substituent ion occupancy. According to these authors [21], the integrated intensity ratios of the (4 0 0)/(3 1 1) and (2 2 0)/(3 1 1) peaks are indices of the extent of substituent ion occupancy in the 8*a* lithium sites. It can be seen from Table 1 that the value of the intensity ratios $I_{4\,0\,0}/I_{3\,1\,1}$ and $I_{2\,2\,0}/I_{3\,1\,1}$ decreased with an increase in the calcination temperature, suggesting that cation disorder gets reduced as the temperature is increased. Thus, samples calcined at high temperatures should be expected to have better electrochemical properties. However, the relatively inferior performance of the sample calcined at 900 °C must be attributed to loss of lithium at high temperatures.

4. Conclusions

A simple and inexpensive method for the preparation of $LiMn_2O_4$ within the matrix of gelled ovalbumin is reported. Water-soluble proteins in ovalbumin upon denaturation forms a matrix of entangled polymeric chains, inside the cavities of which small volumes of precursor salts can be trapped. Upon heat treatment, the dried precursors decompose into nanocrystalline products. Thermal studies showed the formation of $LiMn_2O_4$ at temperatures of about 400 °C. Galvanostatic charge–discharge studies at 0.1 C rate between 3.0 and 4.3 V showed that a sample heat treated at 800 °C for 10 h exhibited the best cycling behavior with a first-cycle capacity of 123.1 mAh/g.

Acknowledgments

The authors acknowledge support received from Dr. Bosco Emmanuel of the Central Electrochemical Research Institute in the execution of this work. Financial assistance for this work was provided by the Department of Science and Technology, Government of India under its SERC scheme.

References

[1] W. Li, J.C. Currie, Morphology effects on the electrochemical performance of $LiNi_{1-x}Co_xO_2$, J. Electrochem. Soc. 144 (1997) 2773–2779.
[2] C.N.R. Rao, Chemical Approaches to the Synthesis of Inorganic Materials, Wiley-Eastern, New Delhi, 1994, p. 28.
[3] A.G. Merzhanov, in: C.N.R. Rao (Ed.), Chemistry of Advanced Materials: A Chemistry for the 21st Century, Blackwell, London, 1993, p. 19.
[4] J. Livage, F. Beteille, C. Roux, M. Chatry, P. Davidson, Sol–gel synthesis of oxide materials, Acta Mater. 46 (1998) 743–750.
[5] G.T.K. Fey, J.G. Chen, Z.F. Wang, H.Z. Yang, T. Prem Kumar, Saturated linear dicarboxylic acids as chelating agents for the sol–gel synthesis of $LiNi_{0.8}Co_{0.2}O_2$, Mater. Chem. Phys. 87 (2004) 246–255.
[6] R.N. Das, P. Pramanik, Low temperature chemical synthesis of nano-size ceramic powder, Br. Ceram. Trans. 99 (2000) 153–158.
[7] R.N. Das, A. Bandyopadhyay, S. Bose, Nanocrystalline α-Al_2O_3 using sucrose, J. Am. Ceram. Soc. 84 (2001) 2421–2423.
[8] J. Jiang, L. Li, Synthesis of sphere-like Co_3O_4 nanocrystals via a simple polyol route, Mater. Lett. 61 (2007) 4894–4896.
[9] S. Dhara, Synthesis of nano-crystalline alumina using egg white, J. Am. Ceram. Soc. 88 (2005) 2003–2004.
[10] B.L. Oser, Hawk's Physiological Chemistry, McGraw Hill Publishers, New York, 1965, p. 1054.
[11] S. Dhara, P. Bhargava, An environmental friendly low cost binder for gelcasting of ceramics, J. Am. Ceram. Soc. 84 (2001) 3048–3050.
[12] S. Dhara, P. Bhargava, A simple direct casting route to ceramic foams, J. Am. Ceram. Soc. 86 (2003) 1645–1650.
[13] K.C. Patil, S.T. Aruna, S. Ekambaram, Combustion synthesis, Curr. Opin. Solid State Mater. Sci. 2 (1997) 158–165.
[14] Y. Gao, J.R. Dahn, Synthesis and characterization of $Li_{1+x}Mn_{2-x}O_4$ for Li-ion battery applications, J. Electrochem. Soc. 143 (1996) 100–114.
[15] C. Masquelier, M. Tabuchi, K. Ado, R. Kanno, Y. Kobayashi, Y. Maki, O. Nakamura, J.B. Goodenough, Chemical and magnetic characterization of spinel materials in the $LiMn_2O_4$–$Li_2Mn_4O_9$–$Li_4Mn_5O_{12}$ system, J. Solid State Chem. 123 (1996) 255–266.
[16] W. Borchardt-Ott, Crystallography, Springer, New York, 1993.
[17] B.D. Cullity, Elements of X-ray Diffraction, Addison-Wesley, New York, 1978, p. 278.
[18] G.T.K. Fey, Y.D. Cho, T. Prem Kumar, A TEA-starch combustion method for the synthesis of fine-particulate $LiMn_2O_4$, Mater. Chem. Phys. 87 (2004) 275–284.
[19] M.M. Thackeray, W.I.F. David, P.G. Bruce, J.B. Goodenough, Lithium insertion into manganese spinels, Mater. Res. Bull. 18 (1983) 461–472.
[20] M.M. Thackeray, Manganese oxides for lithium batteries, Prog. Solid State Chem. 25 (1997) 1–71.
[21] T. Ohzuku, K. Ariyoshi, S. Takeda, Y. Sakai, Synthesis and characterization of 5 V insertion material of $Li[Fe_yMn_{2-y}]O_4$ for lithium-ion batteries, Electrochim. Acta 46 (2001) 2327–2336.
[22] T. Ohzuku, S. Kitano, M. Iwanaga, H. Matsuno, A. Ueda, Comparative study of $Li[Li_xMn_{2-x}O_4$ and LT-$LiMnO_2$ for lithium-ion batteries, J. Power Sources 68 (1997) 646–651.
[23] T. Ohzuku, A. Ueda, Why transition metal (di) oxides are the most attractive materials for batteries, Solid State Ionics 69 (1999) 201–211.
[24] M.M. Thackeray, A Comment on the structure of thin-film $LiMn_2O_4$ electrodes, J. Electrochem. Soc. 144 (1997) L100–L102.